Impact of Coriolis mixing on a two-quasi-neutron isomer in $^{164}Gd_{100}$ and other $N = 100$ isotones

L. Gaudefroy,* S. Péru, N. Arnal, J. Aupiais, J.-P. Delaroche, M. Girod, and J. Libert
CEA, DAM, DIF, F-91297 Arpajon, France

(Received 23 April 2018; published 25 June 2018)

We report on two complementary delayed gamma-ray spectroscopic studies on $^{164}_{64}Gd_{100}$. The nucleus is produced via spontaneous fission of ^{252}Cf sources used in selective experimental setups. An isomeric state at 1095 keV with a half-life of 605 (30) ns is confirmed as well as its decay path toward the ground state band. From comparison to other $N = 100$ isotones and with calculations based on the axially symmetric-deformed quasiparticle random phase approximation (QRPA) using the up-to-date Gogny interaction a 4^- spin and parity is proposed for the isomer. The state is interpreted as a two-quasi-neutron excitation in line with available data for others $N = 100$ isotones. The variation of the lifetime of the isomeric state along the $N = 100$ isotones is interpreted in terms of Coriolis mixing implemented for the first time within axially symmetric-deformed QRPA microscopic calculations.

DOI: 10.1103/PhysRevC.97.064317

I. INTRODUCTION

Spontaneous fission sources produce a large amount of radioactive nuclei therefore offering interesting cost-effective opportunities to study their properties. The major experimental difficulty associated with the use of such sources for performing spectroscopic studies of nonseparated fragments is related to the lack of selectivity inherent to the approach. In conventional experiments performed near accelerators high purity ion beams can be produced and subsequently studied. On the contrary, with spontaneous fission sources the low kinetic energy of the fragments makes it difficult to achieve good identification of produced nuclei and therefore seriously complicates their study. Moreover the few hundreds of exotic nuclei produced in the source and their subsequent radioactive decay generate a huge amount of background signals that have to be dealt with to extract the spectroscopic data of interest associated with a particular fragment. The counterpart of these experimental difficulties is that the full spectroscopy (prompt and delayed) of the produced fragments can potentially be performed using the same experimental setup. In past years, Hamilton and coworkers exploited the great selectivity achieved with triple gamma-ray coincidences detected in the Gammasphere array to obtain valuable spectroscopic data on the prompt decay of band structure of fission fragments produced using various spontaneous fission sources [1]. These measurements exploited the fact that fission fragments are produced at high spin and excitation energy and are therefore perfectly suited for further study of their band structure via the detection of their prompt gamma-decay.

The occurrence of rotational bands in fission fragments is rather common. Indeed most of the produced nuclei lie in regions of the Segré chart where pronounced nuclear deformation is predicted to occur [2]. For some of these regions rapid shape evolution is also predicted [2]. Therefore, not only band structures are expected in these fragments but also shape or K isomers (where K is the projection of the angular momentum onto the z axis in the intrinsic system). While experimental data on the band structure of fission fragments is largely documented in the literature only a limited amount of data are devoted to the study of their isomers [3–5]. We therefore started an experimental project aiming at identifying and, as far as possible, characterizing in terms of structure the isomers populated in fission fragments.

Among the produced fragments, those with $N \simeq 100$ in the vicinity of $Z = 62$ are predicted to be well deformed [6]. This nuclear deformation is proposed to give rise to the observation of the $A \simeq 160$ mass-peak in solar abundance distribution [7]. Several spectroscopic studies in this mass region already provided evidence for important nuclear deformation [8–10]. Isomer spectroscopy has also been used to gain further insight into the structure of these nuclei [11–14]. Their interpretation in terms of K isomer supports the deformation prediction for this mass region. The most recent results [13,14] reported on the existence of an isomeric state in $^{164}_{64}Gd_{100}$. In the present article we report on two complementary experimental approaches and confirm the delayed gamma-ray spectroscopic data on $^{164}_{64}Gd_{100}$ produced in the spontaneous fission of ^{252}Cf. We discuss the systematic occurrence of this isomer in neutron-rich $N = 100$ isotones and in particular on its decay. Recent discussions [13,14] on this decay were essentially limited to a comparison with the approximate rule, first proposed by Löbner [15], on the hindrance factor of K-forbidden transitions. In the present article we offer an original interpretation of the evolution of the lifetime of the isomer along the $N = 100$ isotonic chain based on axially symmetric-deformed quasi-particle random phase calculations on top of which we consider for the first time the effect of Coriolis mixing. This last is a key ingredient in the present interpretation.

In the following we first briefly describe both experimental setups used in this work and then present the corresponding

*laurent.gaudefroy@cea.fr

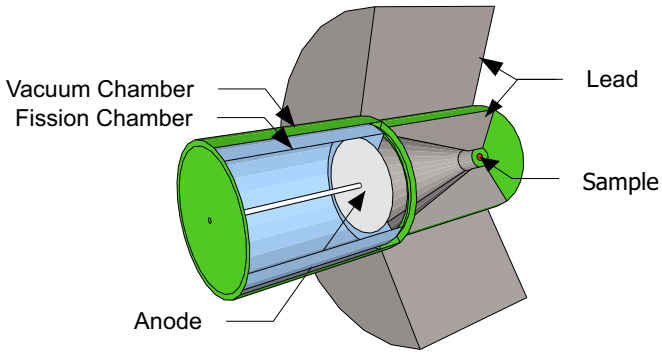

FIG. 1. Scaled schematic view of the experimental setup used in the first experiment. The lead shielding around and inside the vacuum chamber is reported in dark gray. The vacuum chamber is colored in green and the fission chamber is represented in light blue.

results that are compared to available data in other $N = 100$ isotones. The experimental systematics is then discussed in the light of the aforementioned theoretical approach.

II. EXPERIMENTAL SETUPS

The present article is the result of two complementary experiments referred to as experiment or setup one or two in the following. In this section both setups are briefly presented. Figure 1 shows a scaled schematic view of setup 1. An unsealed 6 MBq ^{252}Cf sample electro-plated on a 200-μm-thick platinum foil (reported in red in Fig. 1) is placed into a 140-mm long cylindrical vacuum chamber (50 mm in diameter) operated at a few 10^{-3} mbar. This vacuum chamber, shown in green in Fig. 1, is surrounded by a 70-mm long cylindrical machined lead shielding with a 140-mm outer diameter reported as the outer most dark gray shielding in Fig. 1. Apart from this lead shielding and the germanium detectors used in the experiment the entire setup is encapsulated in the aforementioned vacuum chamber. In front of the ^{252}Cf sample, inside the vacuum chamber, is placed another 70-mm long cylindrical machined lead shielding. This last shielding presents a 10-mm diameter and 10-mm long central hole in front of the ^{252}Cf sample, followed by a 60-mm long 10° conical aperture. Behind this lead shielding is placed a 52-mm diameter 70-mm long fission chamber shown in light blue in Fig. 1. The entrance window of the fission chamber consists of a 2.5-μm metalized polyethylene terephtalate film. The fission chamber is filled with P-10 gas [Ar (90%) + CH_4 (10%)] at 500 mbar continuously flowing at a rate of 0.1 l/min. A high optical transparency (88%) metallic grid stretched in front of the entrance window limits its deformation and avoids its rupture under the effect of the gas pressure. The entrance window of the fission chamber serves as a cathode (not shown on Fig. 1 for more clarity) and is electrically grounded. The anode of the fission chamber, consisting of a 0.5-mm-thick aluminum plate at a +300 V electrical potential, is located only 2 mm behind the cathode. The small anode-cathode gap leads to a time resolution of about 1 ns. The large volume of the fission chamber with respect to the limited active volume (see Fig. 1) is meant for (i) minimizing the pollution of the gas inside the fission chamber by increasing its volume and (ii) minimizing the interaction of the gamma-rays of interest with the flange of the vacuum chamber (also used as the flange of the fission chamber). Outside the vacuum chamber, the fission chamber is surrounded by 8 HPGe coaxial detectors with intrinsic efficiency ranging from 40% to 90% (not shown in Fig. 1). The distance between the entrance window of the Ge detectors and the symmetry axis of the chamber is 100 mm and the orientation of the Ge detectors is perpendicular to the latter axis.

The principle of the measurement in experiment 1 is as follows. When fission occurs at the sample position, prompt gamma-rays, depending of their angle of emission, have to go through at least 70 mm of lead shielding before reaching the Ge detectors. In these conditions, the transmission of prompt gamma-rays below 500 keV is lower than $2 \cdot 10^{-2}$%. After prompt gamma-rays emission, one of the produced fragment might recoil in the vacuum chamber, enter into the fission chamber and induce ionization of the gas. The amplitude of the anode signal, reflecting the fragment energy-loss in the fission chamber, is recorded for each event. The associated timing signal starts a time measurement later stopped by the detection of a delayed gamma-ray emitted by the fragment and detected in the Ge detectors. About $2 \cdot 10^3$ fission fragments enter the chamber per second. Given the mean velocity of the fission fragments their time of flight between the ^{252}Cf sample and the fission chamber amounts to about 5 ns. The trigger of experiment 1 consisted of a coincidence between the fission chamber and at least two γ-rays detected in the Ge detector array.

A detailed description of setup 2 is reported in Ref. [16]. For convenience the main characteristics are recalled here. A 15 kBq ^{252}Cf sample supported by an ultrathin (50-nm thick) carbon backing is loaded in a twin Frisch-grid ionization chamber. Such a thin sample has been produced using the self-transfer technique [16,17] starting from the 6 MBq sample used in experiment 1. The twin ionization chamber consists of two sets of axial chambers sharing a common cathode with a useful diameter of 165 mm. The ^{252}Cf sample is placed at the center of the detector between two conductive plates forming the cathode. The cathode-anode distance is 93 mm. Each of the two anodes are separated from the cathode by stainless-steel mesh serving as Frisch-grids. The anode-grid distance is 13 mm. The detector is encapsulated in a 3-mm thick, 220-mm inner diameter aluminum cylindrical tank. The chamber is filled with P-30 gas at 500 mbar continuously flowing at a rate of 0.05 l/min. The cathode voltage is set to −1600 V while the Frisch-grid is grounded. The anode voltage is set to +1450 V. The ionization chamber is surrounded by ten coaxial HPGe detectors with intrinsic efficiencies ranging from 40% to 80% centered on one half of the ionization chamber.

The principle of the measurement in experiment 2 is as follows. When fission occurs both fragments are detected in coincidence, one in each half of the ionization chamber. A precise measurement of their kinetic energy is performed. The timing signal associated with the cathode starts a time measurement later stopped by the detection of a delayed gamma ray in the Ge array. The range of fission fragments in the chamber amounts to about 4–5 cm, i.e., they are stopped

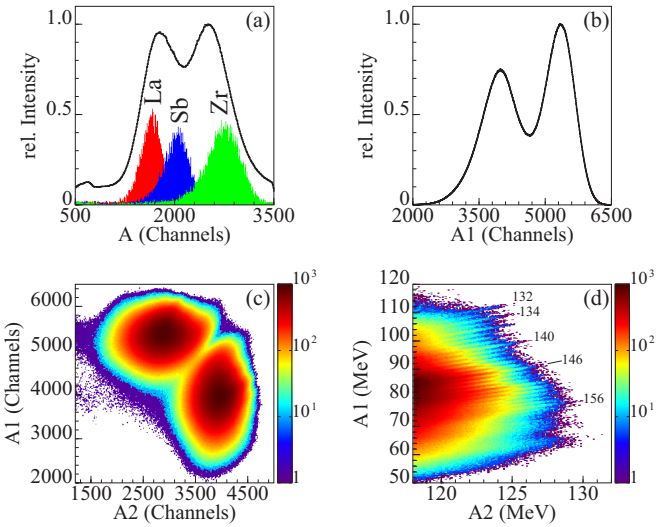

FIG. 2. (a) Normalized anode pulse height measured for fission fragments entering the fission chamber used in Setup 1 (black curve). Arbitrarily scaled distributions gated by the detection of a gamma-ray deexecting isomeric states in ^{146}La, ^{132}Sb, and ^{99}Zr are also reported. (b) Normalized anode pulse height measured with the twin ionization chamber used in Setup 2. (c) Two-dimensional spectrum of anode pulse height measured for fission fragments detected in coincidence in the ionization chamber. (d) Portion of kinetic energies plot showing structures associated with neutron-less fission events.

within less than 5 ns. The trigger of the experiment consisted in a coincidence between both halves of the ionization chamber and at least one delayed γ-ray detected in the Ge detector array.

III. EXPERIMENTAL RESULTS

In this section, we first report on experimental results demonstrating the selectivity achieved with the experimental setups previously presented. Then spectroscopic data obtained for $^{164}_{64}Gd_{100}$ are reported.

Figure 2(a) shows the normalized anode pulse height distribution measured with the fission chamber in experiment 1. The two-hump structure reflects the possibility to distinguish between light and heavy fragments entering the chamber. This is at variance from standard results obtained with such simple detectors that usually hardly separates α-particles from fission fragments (see, for example, Ref. [18]). For the present setup, this useful property stems from the restricted angular dispersion of the fragments entering the chamber. The colored distributions reported in Fig. 2(a) show the anode pulse heights measured in coincidence with γ-rays deexciting isomeric states in ^{146}La [19], ^{132}Sb [20], and ^{99}Zr [20]. As seen from the figure, these three nuclides can partly be distinguished from their pulse heights and a rough mass resolution of $\sigma \simeq 13$ amu is deduced for setup 1. Therefore, gates on mass regions can be applied in the analysis of the data obtained in experiment 1 leading to an increased selectivity of the detection system.

Figure 2(b) shows the normalized anode pulse height distribution measured with the ionization chamber in experiment 2. As expected for a detector meant for precise kinetic energy measurements, the separation between light and heavy fragments, centered on channels 5600 and 3800, respectively, is superior to that obtained with setup 1. The relative amplitudes of the fragment peaks and the valley are in line with those reported in the literature for similar detectors [21,22]. Figure 2(c) shows a two-dimensional spectrum of the anode pulse heights measured in coincidence in both halves of the ionization chamber. One discerns structures in the extreme kinetic energy region $A2 > 4500$ corresponding to the case where the light fragment go through the carbon backing of the ^{252}Cf source. They are associated with neutron-less fission events. These are rare events (global yield of the order of 0.1%) where the primary fragments are produced at an excitation energy lower than their respective neutron separation energies. Neutron emission is therefore energetically forbidden and the conservation of energy and impulsion links the mass of the fragments, M, and their kinetic energies, $A : A_1/A_2 = M_2/M_1$. Figure 2(d) presents a zoomed view of neutron-less structures. Each line in this plot corresponds to a given mass fragmentation with a characteristic slope M_2/M_1. The γ-rays associated with the decay of the 6^+ yrast isomer in ^{134}Te [20] are detected in coincidence with the neutron-less events reported in the line referred to as "134" in Fig. 2(d). Other mass splits are trivially deduced from this reference point. As discussed in details in Ref. [16] the mass resolution obtained for neutron-less fission events amounts to 0.54 amu (FWHM) leading to an energy resolution for fission fragments of about 675 keV.

One notices that no structures are observed in the high kinetic energy region associated with the A_1 anode pulse height in Fig. 2(c). For these events the heavy fission fragment goes through the carbon backing of the ^{252}Cf source and the larger energy-loss and straggling washes out the neutron-less structures. Correcting for the energy-loss of the fragments in the backing of the source makes it possible to observe neutron-less structures in both halves of the chamber as reported in details in Ref. [16].

For spectroscopic purposes it is statistically interesting to reconstruct the mass of the emitting fragments in case of fission accompanied by neutron emission. This postneutron mass can be obtained on an event-by-event basis as a result of an iterative procedure presented in details in Ref. [16] where the resulting postneutron mass resolution is shown to be 4 amu (FWHM).

Figure 3(a) presents the delayed γ-γ spectrum obtained in experiment 1 in coincidence with events in the fission chamber with anode pulse heights ranging from channel 1150 to channel 1750 [see Fig. 2(a)]. This last condition selects the heaviest fission fragments produced in the fission of ^{252}Cf. The gamma transition at 168 keV is observed in coincidence with a 854 keV γ-ray. Given the mass-resolution in setup 1 it is not possible to deduce which fragment emitted the observed gamma-rays.

These γ-lines are also observed in the single delayed gamma-ray spectrum obtained with setup 2 and reported in Fig. 3(b). This spectrum is measured in coincidence with fission events where the postneutron mass of the heavy fragment lies in the range [163–165] and the total kinetic energy for the event is larger than 175 MeV. This last condition improves the signal-to-noise ratio. The structure observed around 700 keV arises from the interaction of fission neutrons with the Ge detectors. As a result of a better selectivity in

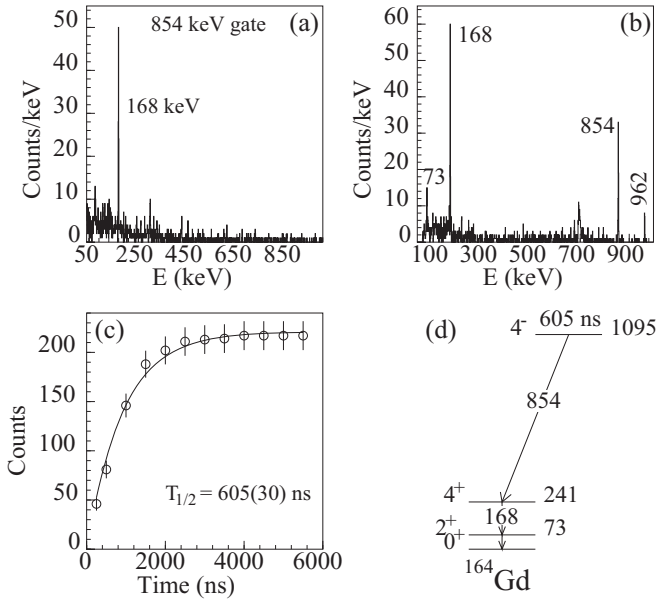

FIG. 3. (a) Gamma-ray spectrum measured in coincidence with a heavy fragment in the fission chamber in Setup 1 and in coincidence with a delayed γ-ray at 854 keV. (b) Single delayed γ-ray spectrum obtained for fission events with a heavy fragment postneutron mass of 164 and TKE > 175 MeV. (c) Time pattern associated with the 168 keV γ ray. (d) Deduced partial level scheme for ^{164}Gd.

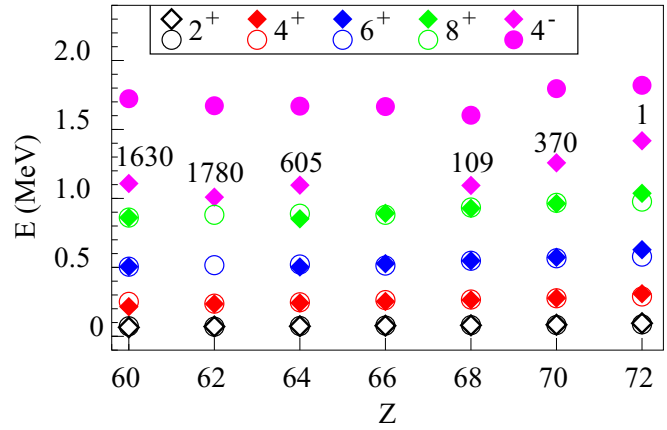

FIG. 4. Low-energy level structure for $N = 100$ isotones discussed in the text. Diamond (circle) symbols show experimental (theoretical) data. The number reported on top of the experimental 4^- point corresponds to the measured half-live (in ns) of the isomer. The theoretical $(2–8)^+$ excitation energies are calculated within the 5DCH approach, while the theoretical 4^- energy, shown as filled pink circle, is the result of QRPA calculations.

experiment 2 as compared to that of experiment 1 one observes an additional transition at 73 keV in Fig. 3(b). Moreover a 962-keV transition is also observed in the single γ-ray spectrum obtained in experiment 2 and not in the coincidence spectrum of experiment 1. These experimental results are in line with those recently reported for $^{164}Gd_{100}$ [13,14], with a delayed transition at 854 keV decaying from an isomeric state at 1095 keV towards the 4_1^+ state lying at 241 keV. This last decays by a 168 keV towards the 73 keV 2_1^+ state.

Figure 3(c) shows the cumulative number of counts observed in the 168 keV line as a function of time after fission events. The half-life of the isomeric state deduced from the adjustment of the data [black curve in Fig. 3(c)] is $T_{1/2} = 605$ (30) ns. The error bar arises from statistics only. The mean value determine for the present half-life is slightly larger than those previously reported [13,14], it is, however, fully in agreement with the last of these within the quoted error bars. Figure 3(d) summarizes the experimental results obtained in this work for ^{164}Gd. It is worth mentioning that the evaluated yield for $^{164}Gd_{100}$ amounts to only $2.95 \cdot 10^{-2}$% [23]. Together with the quality of the single γ-ray spectrum reported in Fig. 3(b), comparable to that of the coincidence spectrum shown in Fig. 3(a) or to that reported in Refs. [13,14] using the BigRIPS fragment separator at Riken, it demonstrates the good selectivity achieved with the twin ionization chamber used in setup 2. We mention here that the 962 keV transition observed in Fig. 3(b) cannot be placed in the present level scheme using our experimental results solely. However, it is proposed in Refs. [13,14] to belong to an additional decay branch of the isomeric state. In this decay branch, a low-energy transition (60 keV) not observed in the present work links the isomer to a proposed 3^+ state at 1034 keV (member of the $K = 2$ γ-band) that subsequently decays by a 962 keV transition toward the 2_1^+ state. This is compatible with the observation of the 962 keV line only in the single γ spectrum of experiment 2 due to the magnitude of the conversion coefficients associated with the low energy transitions that should be observed in coincidence.

IV. DISCUSSION

In this section the experimental results obtained in the present work are compared to available data for others $N = 100$ nuclei as well as to theoretical model calculations. The discussion is then focused on the variation of the lifetime of the isomer of interest along the $N = 100$ chain. We include in our discussion all the even-even $N = 100$ nuclei between $^{160}_{60}$Nd and $^{170}_{70}$Yb, those later being the lightest and the heaviest nuclei for which a similar isomer has been reported. We also include $^{172}_{72}$Hf in the discussion. For that nucleus the state of interest is reported with a lifetime significantly shorter than that for other isomers in the systematics. The transition between long and short lifetimes will be studied.

A. Experimental systematics

Figure 4 shows the low energy level structure systematic of even-even $N = 100$ isotones including the present results for $^{164}_{64}Gd_{100}$. The diamond symbols correspond to experimental data. As can be deduced from their ground state (GS) rotational bands, reported in Fig. 4 up to the 8^+ state when available, all the considered isotones present very similar yrast structure and are good rotors with a ratio of their 4_1^+ to 2_1^+ excitation energies, R_{42}, close to 3.3. The existence of a 4^- isomeric state at an excitation energy of ranging from 1 MeV to about 1.5 MeV is also a common feature for $N = 100$ isotones as seen from the pink diamond symbols in Fig. 4. The spin and parity of this isomer has been well established at the stability

line, for $Z = 68$ and $Z = 70$, from transfer reaction [24], magnetic moment measurement [25], and angular correlation or conversion electron spectroscopy [26–28]. In neighboring $N = 100$ nuclei, the proposed spin and parity of the isomer has been mainly justified based on the systematic of $N = 100$ isotones and from the comparison with Nilsson-model-type calculations. This last predicts a $K^\pi = 4^-$ state as the first two-quasi-particle (2qp) excitation in the considered isotone. Theoretically this 4^- state is built on the $\nu(1/2[521] \otimes 7/2[633])$ two-quasi-particle excitation in agreement with experimental results at the stability line [24–27].

When observed experimentally, the 4_1^- isomer mainly decays toward the 4_1^+ of the GS band, except for $^{168}_{68}$Er where the decay toward the 3^+ state belonging to the γ-band is more intense. At the stability line, for $Z = 68$ and $Z = 70$, a $E1$ multipolarity is measured for the $4_1^- \rightarrow 4_1^+$ transition [26,28]. As such, the isomeric nature of the 4_1^- state stems from the K hindrance associated with its main decay-branch.

Strikingly, although the low-lying structure of the considered $N = 100$ isotones looks very similar, the half-life of the 4^- isomer (reported in ns in Fig. 4) shows large and nonmonotonic variations along the isotopic chain. In the following the origin of the evolution of this half-life is discussed.

B. 5DCH description

First, the GS band of considered $N = 100$ isotones has been calculated using the generator coordinate method within the Gaussian overlap approximation to perform configuration mixing of deformed Hartree-Fock-Bogoliubov (HFB) states. This approach referred to as five-dimensional collective Hamiltonian (5DCH) explicitly treats all axial and triaxial quadrupole degrees of freedom [29–31]. This model has already demonstrated its reliability for the description of nuclear properties over the nuclear chart [31–36]. In this work, we use the Gogny D1M [37] effective interaction and checked that excitation energies do not significantly differ from those obtained with the D1S interaction [38,39]. For the present calculations HFB equations are solved in a triaxial harmonic oscillator (HO) basis including 12 major shells. The 5DCH results are reported as a set of open circles in Fig. 4. An excellent agreement is obtained with available data including the most recent ones reported at $Z = 62$ [13]. A similar agreement on the excitation energies of the levels belonging to the ground-state band is common in the literature [13] for these good axially deformed rotors. All considered isotones are calculated to be prolate with a mean axial deformation of about $< \beta >= 0.35$. Members of the GS band show pure $K = 0$ wave functions. Admixtures of higher K values are less than 1%, and hence the impact of the triaxial degree of freedom is calculated to be negligible for the considered states.

C. QRPA description

To gain a deeper understanding of the structure of the isomer of interest in $N = 100$ isotones, calculations within the quasiparticle random phase approximation (QRPA) framework have been performed. Here we just give a brief summary of the principle of the calculations and we refer the reader to Refs. [40–42] for more details. The present QRPA approach is based on axially symmetric-deformed HFB calculations using the D1M Gogny effective interaction. HFB equations are solved in a finite HO basis containing 12 major shells in cylindrical coordinates. The solutions of HFB equations are the quasiparticle states that are then used to define two-quasi-particle (2qp) excitations. Coherent superposition of 2qp excitations defines the QRPA phonons that describe the band-heads in the considered even-even nuclei for which K, the projection of the angular momentum onto the z axis in the intrinsic system, and parity are good quantum numbers.

The present QRPA calculations, free from any adjustable parameter, predict a low-lying $K^\pi = 4^-$ excitation for the considered nuclei at the same deformation than that for the GS band. For all isotones this state is mainly built on the $\nu(1/2[521] \otimes 7/2[633])$ configuration originating from the $3p_{3/2}$ and $1i_{13/2}$ spherical neutron orbits. As already stated, this is in line with the interpretation of the structure of the isomer of interest previously reported [13,14]. The excitation energies of the calculated 4^- states are reported as a set of filled pink circles in Fig. 4. The calculations overestimate the excitation energy of the isomer by about 500 keV, a level of agreement already observed in other regions of the nuclear chart with the present QRPA approach free from adjustable parameters [43]. One notices that more flexible theoretical approaches might provide a comparable [13] or even better [14] agreement with experimental excitation energies in this mass region. As a result of the conserved symmetries within our QRPA approach the decay of the $K^\pi = 4^-$ towards the $K^\pi = 0^+$ GS band can only occur via transitions of multipolarity larger or equal to 4 leading to a corresponding lifetime of the order of a few tens of hours. Some form of K mixing must therefore exist in order to enable K-forbidden transitions between the isomer and the lower-lying states.

A possible reason for K-mixing in the wave function of the isomer could come from triaxial shape fluctuation [44]. However, this option can most likely be ruled out since no sign of the impact of triaxial shapes is calculated in the low-lying structure of the isotones of interest, as stated in the previous subsection. Instead we considered the effect of the Coriolis interaction on the states of interest in $N = 100$ isotones. Such an approach has already been applied successfully in the past to describe the properties of the band built on the $K^\pi = 4^-$ isomer at the stability line in ^{170}Yb [26]. The interaction only mixes states differing by one unit in their K values. The basic idea of the present calculation is therefore that the $K = 4$ isomer can mix with a close-lying $K = 3$ state; the last being mixed with a $K = 2$ state itself mixed with a $K = 1$ state, and so on. Following this successive mixing small admixtures of low K values can appear in the wave function of the 4^- isomer and open the way for a faster decay toward low-lying states. To induce such a mixing, $J^\pi = 4^-$ states with $K = 0$, 1, 2, and 3 should lie at an excitation energy close to that of the isomer and within the range of the Coriolis force. Figure 5 displays the excitation energy of the first $J^\pi = 4^-$ states with $K = 0$, 1, 2, 3, and 4 calculated for the $N = 100$ isotones. To determine these energies, a QRPA calculation first provided the excitation energies of the $K = 0$, 1, 2, 3, and 4 band-heads as well as the decomposition of their wave functions in terms of

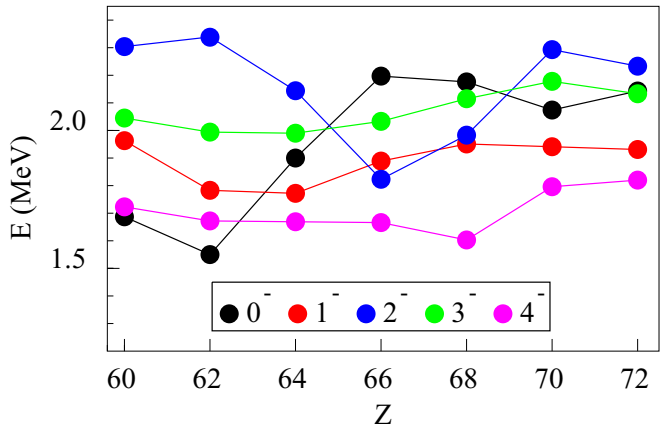

FIG. 5. Excitation energy of the $J^\pi = 4^-$ states built on $K = 0$, 1, 2, 3, and 4 QRPA band heads for $N = 100$ isotones of interest. States are labeled by their K values.

quasiparticle configurations. Blocked HFB calculations have therefore been used to determine the moment of inertia of the rotational bands built on the band-heads by considering the main components (larger than 10%) of their wave functions. Then the standard rotational formula has been used in order to deduce the excitation energies reported in Fig. 5.

The matrix element of the Coriolis interaction, H_C, acting between QRPA states just discussed and labeled by their K values can be written [45] as

$$\langle K|H_C|K+1\rangle = \frac{-\hbar^2}{2I}\sqrt{(J-K)(J+K+1)}\,\langle K|\mathbf{j}_-|K+1\rangle, \quad (1)$$

where $\hbar^2/2I$ is the inertia parameter; J is the spin of the considered state (here $J = 4$); $\mathbf{j}_-$ is the decrease operator acting on the particle angular momentum. The Coriolis interaction is expected to be rather important in the present case where the configuration of the isomer involves the high angular momentum $1i_{13/2}$ unique parity orbit [46]. For all the considered isotones we find, applying Eq. (1), that the intensity of the Coriolis interaction ranges from few keVs up to about 100 keV depending on the coupled states. This intensity is reduced as compared to its maximum expectation value [46] because of the pairing factors and the fractionation of the QRPA wave functions.

To perform mixing between the various $J^\pi = 4^-$ states, a tridiagonal energy matrix is built where the diagonal elements consist of the excitation energies of the states displayed in Fig. 5 and the subdiagonal elements are the matrix elements of the Coriolis interaction given by Eq. (1). The eigenvectors and eigenvalues of the energy matrix provide the mixing amplitudes and the excitation energy of the mixed states. The mixing amplitudes calculated for the 4^- isomer are gathered in Table I for all the considered isotones. As seen from the table, the $J^\pi = 4^-$ states remain rather pure with the amount of mixing of the order of 10^{-3}. Such low mixing amplitudes are expected when the energy spacings between the unperturbed states are larger than the strength of the mixing interaction.

TABLE I. Mixing amplitudes of the considered 4^- states.

Z	$K=0$	$K=1$	$K=2$	$K=3$	$K=4$
60	0.0000	0.0001	0.0171	0.0005	0.9998
62	0.0000	0.0001	0.0178	0.0005	0.9998
64	0.0005	0.0004	0.0236	0.0005	0.9997
66	0.0000	0.0022	0.0048	0.0324	0.9995
68	0.0002	0.0021	0.0069	0.0329	0.9994
70	0.0015	0.0011	0.0500	0.0108	0.9987
72	0.0026	0.0509	0.0086	0.0017	0.9987

Since the mixing is weak, the excitation energies of the mixed states are only shifted by few keV.

Combining the mixing amplitudes with the reduced transition rates calculated within our QRPA approach between the unperturbed band heads and the GS band, we finally deduced the lifetime of the isomer. The calculated half-lives are reported in Table II together with the contributions, in percentage, of the $E1$, $M2$, and $E3$ multipolarities to the total transition rate. While the agreement is not yet perfect, one sees a great improvement in the comparison to the experimental data. It is noteworthy that minuscule admixtures in the wave function of the state, as reported in Table I, allow to reduce the half-lives of interest by several orders of magnitude (from few hours for allowed transitions with multipolarities larger than 4 down to the values reported in Table II). One notices that for the particular case of $^{168}_{68}$Er, the main decay branch for the 4^- isomer is experimentally observed towards the γ-band and is not considered in the present calculations. The experimental counterpart of the partial half-life calculated here amounts to about 1000 ns for this nucleus.

An additional noticeable result, seen in Table II, is that the decay of the isomer in the lightest isotones, i.e., the isotones where the considered lifetime is the longest, is mainly of $E3$ nature while for the heaviest isotones, with the shortest lifetime, the decay is dominated by $E1$ transition rates. The transition between both groups of nuclei is driven by the competition between the mixing of $K = 1$ or $K = 2$ components. Even if the mixing amplitudes for the $K = 3$ component might seem sizable in some isotones (see Table I), the associated transition rates are low and therefore this component does not

TABLE II. Calculated half-lives, $T_{1/2}^{QRPA}$, for the considered $J^\pi = 4^-$ state compared with the experimental value, $T_{1/2}^{Exp}$, when available. The theoretical contributions of the $E1$, $M2$, and $E3$ multipolarities to the decay of the 4^- state are also reported in percentages.

Z	$E1$	$M2$	$E3$	$T_{1/2}^{QRPA}$ (ns)	$T_{1/2}^{Exp}$ (ns)
60	7	2	90	6970	1630(210)
62	6	2	92	11105	1780(70)
64	37	1	62	3980	605(30)
66	99	0	1	285	
68	99	0	1	365	109(7)
70	60	0	40	260	370(15)
72	100	0	0	1.5	$\simeq 1$

contribute significantly to the total transition rate. Looking at Fig. 5, one can get an intuitive understanding of the relative evolution of $K = 1$ and $K = 2$ mixing in the wave functions of interest. For the heaviest isotones, the *successive* energy spacings between $K = 1$, 2, and 3 states is smaller than that observed for the lightest isotones, therefore leading to a larger mixing in the final wave function of the isomer. For example, $K = 1$, 2, and 3 states lie within about 200 keV at $Z = 66$ and $Z = 68$ leading to a large amount of $K = 1$ admixtures and short lifetimes, as seen from Tables I and II. Similarly, at $Z = 72$ all the considered states (see Fig. 5) lie within the smallest energy window, and the amount of $K = 1$ component in the final wave function of the 4^- state reaches its maximum value. As a result, the state is no longer an isomer with an experimental lifetime in the nanosecond range, well accounted for by present calculations. On the contrary, at $Z = 60$ and $Z = 62$, the energy spacing between $K = 1$ and $K = 2$ states on the one hand and $K = 2$ and $K = 3$ states on the other hand are the largest therefore inhibiting the mixing with low K values in the final wave function, resulting in a longer lifetime.

Even though the result of the diagonalization of the full energy matrix is more complex than successive two states arguments and even though the evolution of the Coriolis matrix elements and the variation of the individual transition rates between the considered isotones has been neglected in this intuitive reasoning, it provides the basic idea for the understanding of the evolution of the lifetime of the $J^\pi = 4^-$, $K = 4$ isomer in $N = 100$ isotones.

V. CONCLUSION

In summary, we report on two complementary experiments aiming at studying the delayed γ-ray spectroscopy of non-separated fission fragments produced in the spontaneous fission of ^{252}Cf. An isomeric state has been reported in ^{164}Gd$_{100}$ and its decay path toward the ground state band is characterized. The present results, obtained with a relatively simple and cost-effective experimental approach, are in line and confirm those recently obtained at Riken using the BigRIPS fragment separator. From systematics of $N = 100$ isotones and comparison to axially symmetric-deformed QRPA calculations the isomeric state is proposed to be a $K^\pi = 4^-$ state mainly built on the $\nu(1/2[521] \otimes 7/2[633])$ two-quasi-particle configuration, in line with previous interpretations of the structure of the isomer in $N = 100$ isotones. The evolution of the half-life of the 4^- isomer along the $N = 100$ isotones has been quantitatively discussed within the QRPA framework. Coriolis mixing of low K components is proposed to be the key ingredient for the understanding of this evolution. A satisfactory reproduction of the experimental trend is obtained in the present work due to tiny admixtures brought in the wave function of the isomer by the Coriolis interaction. The 4^- isomer in the heaviest $N = 100$ isotones is found to mainly decay via $E1$ transition towards the ground state band with a typical lifetime of the order of hundreds of nanoseconds. In lighter isotones, because of the evolution of the nature and the amount of admixture in the wave function of interest, the decay mainly proceed via $E3$ transitions resulting in a longer lifetime of the order of few microseconds.

The present work is the first one where K-mixing is performed on top of axially symmetric-deformed QRPA approach. Further systematic theoretical studies are envisioned in the near future. Experimentally, it could be interesting to confirm the present interpretation and, for example, to observe the predicted isomer in $^{166}_{66}$Dy. The study of the rotational bands built on top of the isomers could also provide valuable information on their nuclear structure.

ACKNOWLEDGMENTS

L.G. thanks A. Chatillon for her technical support with the data acquisition system used in experiment 2 and P. Marini for a critical reading of the manuscript.

[1] J. H. Hamilton *et al.*, Prog. Part. Nucl. Phys. **35**, 635 (1995).
[2] S. Hilaire and M. Girod, Eur. Phys. J. A **33**, 237 (2007).
[3] W. John *et al.*, Phys. Rev. C **2**, 1451 (1970).
[4] R. E. Sund *et al.*, Phys. Rev. C **10**, 853 (1974).
[5] R. G. Clark *et al.*, in *Proceedings of a Symposium on Physics and Chemistry of Fission* (Rochester, New York, 1973), Vol. II, p. 221.
[6] L. Satpathy and S. K. Patra, J. Phys. G: Nucl. Part. Phys. **30**, 771 (2004).
[7] R. Surman, J. Engel, J. R. Bennett, and B. S. Meyer, Phys. Rev. Lett. **79**, 1809 (1997).
[8] E. F. Jones *et al.*, J. Phys. G: Nucl. Part. Phys. **30**, L43 (2004).
[9] P.-A. Söderström *et al.*, Phys. Rev. C **81**, 034310 (2010).
[10] V. Karayonchev, J. M. Régis, J. Jolie, A. Blazhev, R. Altenkirch, S. Ansari, M. Dannhoff, F. Diel, A. Esmaylzadeh, C. Fransen, R.-B. Gerst, K. Moschner, C. Müller-Gatermann, N. Saed-Samii, S. Stegemann, N. Warr, and K. O. Zell, Phys. Rev. C **95**, 034316 (2017).
[11] Z. Patel *et al.*, Phys. Rev. Lett. **113**, 262502 (2014).
[12] E. Ideguchi *et al.*, Phys. Rev. C **94**, 064322 (2016).
[13] R. Yokoyama, S. Go, D. Kameda, T. Kubo, N. Inabe, N. Fukuda, H. Takeda, H. Suzuki, K. Yoshida, K. Kusaka, K. Tanaka, Y. Yanagisawa, M. Ohtake, H. Sato, Y. Shimizu, H. Baba, M. Kurokawa, D. Nishimura, T. Ohnishi, N. Iwasa, A. Chiba, T. Yamada, E. Ideguchi, T. Fujii, H. Nishibata, K. Ieki, D. Murai, S. Momota, Y. Sato, J. W. Hwang, S. Kim, O. B. Tarasov, D. J. Morrissey, B. M. Sherrill, G. Simpson, and C. R. Praharaj, Phys. Rev. C **95**, 034313 (2017).
[14] Z. Patel *et al.*, Phys. Rev. C **96**, 034305 (2017).
[15] K. E. Löbner, Phys. Lett. B **26**, 369 (1968).
[16] L. Gaudefroy *et al.*, Nucl. Instrum. Methods A **855**, 133 (2017).
[17] S. Pauker and N. H. Steiger-Shafrir, Nucl. Instrum. Methods A **91**, 557 (1971).
[18] J. Taieb *et al.*, Nucl. Instrum. Methods A **833**, 1 (2016).
[19] J. K. Hwang, A. V. Ramayya, J. Gilat, J. H. Hamilton, L. K. Peker, J. O. Rasmussen, J. Kormicki, T. N. Ginter, B. R. S. Babu, C. J. Beyer, E. F. Jones, R. Donangelo, S. J. Zhu, H. C. Griffin, G. M. TerAkopian, Y. T. Oganessian, A. V. Daniel, W. C. Ma,

P. G. Varmette, J. D. Cole, R. Aryaeinejad, M. W. Drigert, and M. A. Stoyer, Phys. Rev. C **58**, 3252 (1998).
[20] Evaluated Nuclear Structure Data File, http://www.nndc.bnl.gov/ensdf/.
[21] A. Oed *et al.*, Nucl. Instrum. Methods **205**, 455 (1983).
[22] F.-J. Hambsch *et al.*, Nucl. Instrum. Methods **361**, 257 (1995).
[23] A. C. Wahl, At. Data Nucl. Data Tables **39**, 1 (1988).
[24] R. A. Harlan and R. K. Sheline, Phys. Rev. **160**, 1005 (1967).
[25] A. Furusawa, M. Kanazawa, and S. Hayashibe, Phys. Rev. C **21**, 2575 (1980).
[26] P. M. Walker *et al.*, Nucl. Phys. A **365**, 61 (1981).
[27] D. E. Archer, M. A. Riley, T. B. Brown, D. J. Hartley, J. Döring, G. D. Johns, J. Pfohl, S. L. Tabor, J. Simpson, Y. Sun, and J. L. Egido, Phys. Rev. C **57**, 2924 (1998).
[28] J. Jursík and V. Zvolská, Nucl. Phys. **86**, 405 (1966).
[29] J. Libert, M. Girod, and J.-P. Delaroche, Phys. Rev. C **60**, 054301 (1999).
[30] M. Girod and B. Grammaticos, Phys. Rev. C **27**, 2317 (1983).
[31] G. F. Bertsch, M. Girod, S. Hilaire, J.-P. Delaroche, H. Goutte, and S. Péru, Phys. Rev. Lett. **99**, 032502 (2007).
[32] A. Obertelli, S. Péru, J.-P. Delaroche, A. Gillibert, M. Girod, and H. Goutte, Phys. Rev. C **71**, 024304 (2005).
[33] S. Péru, M. Girod, and J. F. Berger, Eur. Phys. J. A **9**, 35 (2000).
[34] M. Girod, J.-P. Delaroche, A. Görgen, and A. Obertelli, Phys. Lett. B **676**, 39 (2009).
[35] L. Gaudefroy, A. Obertelli, S. Péru, N. Pillet, S. Hilaire, J.-P. Delaroche, M. Girod, and J. Libert, Phys. Rev. C **80**, 064313 (2009).
[36] J.-P. Delaroche, M. Girod, J. Libert, H. Goutte, S. Hilaire, S. Peru, N. Pillet, and G. F. Bertsch, Phys. Rev. C **81**, 014303 (2010).
[37] S. Goriely, S. Hilaire, M. Girod, and S. Péru, Phys. Rev. Lett. **102**, 242501 (2009).
[38] J. F. Berger, M. Girod, and D. Gogny, Nucl. Phys. A **502**, 85c (1989); Comput. Phys. Commun. **63**, 365 (1991).
[39] J. Dechargé and D. Gogny, Phys. Rev. C **21**, 1568 (1980).
[40] S. Péru and H. Goutte, Phys. Rev. C **77**, 044313 (2008).
[41] S. Péru and M. Martini, Eur. Phys. J. A **50**, 88 (2014).
[42] M. Martini, S. Péru, S. Hilaire, S. Goriely, and F. Lechaftois, Phys. Rev. C **94**, 014304 (2016).
[43] A. Corsi *et al.*, Phys. Lett. B **743**, 451 (2015).
[44] F. G. Kondev, G. D. Dracoulis, and T. Kibédi, At. Data Nucl. Data Tables **103–104**, 50 (2015).
[45] F. S. Stephens and R. S. Simon, Nucl. Phys. A **183**, 257 (1972).
[46] F. S. Stephens, Rev. Mod. Phys. **47**, 43 (1975).